Catalysis Today 153 (2010) 176–183

Contents lists available at ScienceDirect

Catalysis Today

journal homepage: www.elsevier.com/locate/cattod

Effect of manganese oxide catalyst on the dielectric barrier discharge decomposition of toluene

Yufang Guo[a,*], Xiaobin Liao[a,b], Jianhua He[a], Weijian Ou[a], Daiqi Ye[b]

[a] College of Environmental Science and Engineering, Guangzhou University, 230 Wai Huan Xi Road, Guangzhou, Guangdong 510006, China
[b] College of Environmental Science and Engineering, South China University of Technology, 382 Wai Huan Dong Road, Guangzhou, Guangdong 510006, China

ARTICLE INFO

Article history:
Available online 14 April 2010

Keywords:
Dielectric barrier discharge
Catalyst
Hydroxyl radical
Toluene removal

ABSTRACT

Effect of manganese oxide catalyst on the toluene removal efficiency, byproducts inhibition and hydroxyl radical (HO*) formation were studied in dielectric barrier discharge (DBD) system. It was found that with MnO_X catalyst, the toluene removal efficiency was nearly two times than that of without catalyst, but the HO* yield in gas streams was only one eighth of that without catalyst at a specific energy density (SED) of 50 Wh/m^3. Meanwhile, byproducts of O_3 and NO_x were in much lower concentrations with the catalyst. The experiment about quantities of HO* radicals in the gas phase and on the surface of catalyst proves that HO* would be attached on the surface of catalyst. In order to investigate the performance of MnO_X catalyst, a characterization of the catalyst was performed by BET surface area detector, X-ray photoelectron spectroscopy (XPS) and temperature programmed reduction (TPR). The results of XPS suggested that various oxygen species and some compounds containing N element deposited on the catalyst after plasma reaction. As a result, catalytic control in situ could be one of the most effective approaches to increase toluene removal efficiency and achieve a higher selectivity of CO_2.

1. Introduction

The emission of volatile organic compounds (VOCs) from various industrial processes is one of the most important sources for air pollution. VOCs are damaging for both human health and environment, either directly for their toxicity and malodorous nature or indirectly as ozone and smog precursors [1]. Non-thermal plasma (NTP) was thought to be an available way to decompose diluted VOCs. While NTP alone has many disadvantages, such as low energy efficiencies, poor selectivity to carbon dioxide and byproduct formation, an attempt to overcome these limitations is a combination of NTP method with catalysts [2–4]. Various catalysts such as noble metals, metal oxides or mixture were investigated in NTP reaction [4–6].

Hydroxyl radical (HO*) was supposed to be a very important reactive species because it was responsible for the oxidation of VOCs and affected their removal efficiency in plasma system [7–9]. But seldom researches were concerned about the formation of HO* in non-thermal plasma system with/without catalyst. In addition, due to the lives of plasma radicals are very short (radical life based on self-recombination is 10^{-9} s), the detecting work becomes difficult. In the last few years, some researchers investigated several ways to study the radicals in plasma reaction. For example, laser induced fluorescence (LIF) has been already employed by authors [10–15] for studying NO removal process in various non-thermal plasma reactors. Recently, several researchers succeeded in measuring the OH radicals using LIF technique in the pulsed corona discharges [16–20]. Machala et al. [21] demonstrated several ways of use of the UV–vis optical emission spectroscopy (OES) for the diagnostics of atmospheric pressure air and nitrogen plasmas. However, in these articles the real amount of radicals had not been affirmed.

In this paper, a film impregnated with salicylic acid (SAL) was used to collect OH radical in the DBD reaction. Manganese oxide was used as a catalyst and it was placed in the discharge area of a wire-plate dielectric barrier discharge reactor. The combination effect of plasma and manganese oxide catalyst was studied on the toluene removal efficiency, byproducts inhibition and hydroxyl radical formation. In addition, a characterization of the catalyst was performed by BET, XPS and TPR.

2. Experimental

2.1. Experimental set up

A schematic diagram of the experimental system is shown in Fig. 1. The experiments were performed at room temperature and atmospheric pressure. The apparatus mainly includes a gas sup-

* Corresponding author.
E-mail address: yufanguo@hotmail.com (Y. Guo).

0920-5861/$ – see front matter © 2010 Elsevier B.V. All rights reserved.
doi:10.1016/j.cattod.2010.03.024

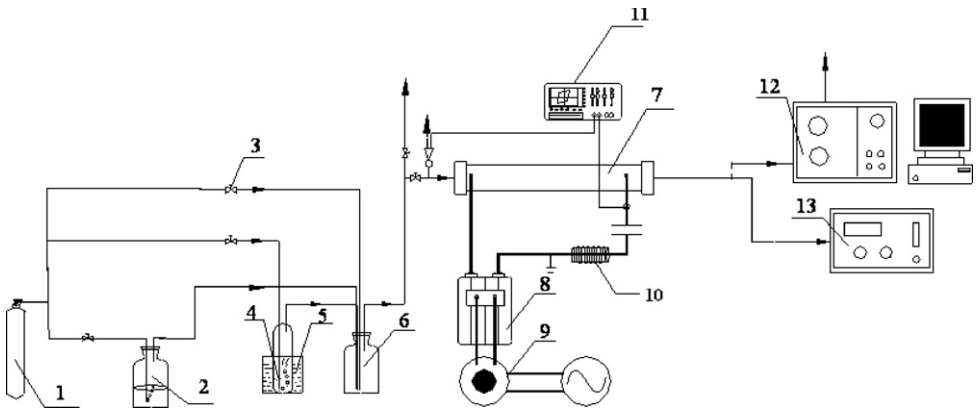

Fig. 1. Schematics diagram of the experiment. (1) Dry gas cylinder, (2) bubbling for water vapor preparation, (3) mass flow controller, (4) bubbling for toluene preparation, (5) water bath for toluene generation, (6) buffer, (7) DBD reactor, (8) ac transformer, (9) booster, (10) resistance, (11) oscillograph, (12) gas chromatogram, and (13) ozone analyzer.

plying and regulating system, a self-made DBD reactor with power supply system and a gas analysis system. The initial toluene concentrations were controlled from 200 mg/m^3 to 800 mg/m^3. The gaseous toluene was regulated by controlling the air flow rate from gas cylinder through pure toluene liquid (>99.5%) which was kept in a water bath ($T = 25 \pm 1\,^\circ$C). After passing through a mixing chamber, the feeding gases entered the DBD reactor. The gas flow rates were controlled at a range of 150–450 ml/min. The feeding gases with different humidities, which were measured by a humidity meter (Center 310, Qunte), were simulated by controlling water bubbling system.

Gas samples were obtained from the effluent by an auto-sampler and were analyzed on-line. Toluene and other volatile organic compounds were analyzed by a gas chromatograph (GC-7890II, Tianmei) equipped with a hydrogen flame ionization detector (FID) and a DB-5MS capillary column (30 m × 0.25 mm × 0.25 mm) heated at 80 °C. The concentration of CO and CO_2 in the discharge was measured by a CO analyzer (TX2000, Oldham) and a CO_2 detector (GXH-3010E, Huayun), respectively. The concentration of ozone was monitored by an ozone analyzer (DCS-1, Lida). The formation of NO in the discharge was checked with a NO analyzer (PGM-1140, Rae), and a NO_2 analyzer (PGM-1150, Rae) was used for that of NO_2.

2.2. DBD reactor and power supply system

Fig. 2 shows the structure of a wire-plate DBD reactor in the reaction. Two epoxy resin boards (200 mm × 45 mm × 0.8 mm) were used to form the reactor walls and acted as dielectric barriers (the dielectric constant $\varepsilon = 3.6$). A high-voltage electrode was made of brass wire with 0.6 mm in diameter. This electrode was shaped into a spiral in order to increase the energy density in the reaction volume. The wire-to-wire distance was 8 mm. Two grounded electrodes were made of copper nets and fixed on the two sides of a middle epoxy resin board. The total length of the reactor was 200 mm, while the effective length was 150 mm. When no catalyst was used, the gap between the high-voltage electrode and the grounded electrode was 8 mm, resulting in a cross-sectional area for the flow channel of 400 mm^2 and a reaction volume of 60 cm^3. To add a catalyst, it was supported by two pieces of nickel foam (150 mm × 25 mm × 2 mm) fixed to the grounded electrodes. This produced a gap of 6 mm, a cross-sectional area for the flow channel of 300 mm^2 and a reaction volume of 45 cm^3.

High-voltage power was supplied by a booster (0–250 V) cooperated with a high-voltage AC transformer (5–25 kHz, 30 kV) in series. In this experiment the frequency was controlled at 9.512 kHz. The applied voltage was measured by a high-voltage probe (P6015, Tektronix) and a digital oscillogragh (TDS1002, Tektronix) was used to measure the voltage and current deposited to the reactor. The input power included the discharge power (the power deposited to the reactor) and the power consumption of the transformer and the circuit. The discharge power was calculated from the applied voltage and the reactor current. In this experiment, the discharge power was proportional to the input power by a factor of 0.5–0.63 in the DBD–catalyst system and by a factor of approximately 0.35 in the DBD system.

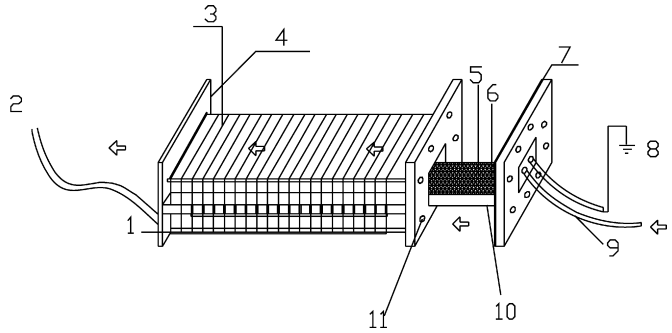

Fig. 2. Structure of the DBD reactor with catalyst. (1) Positive electrode, (2) polyethylene tube (gas out), (3) brass wire, (4) epoxy resin board (1 mm), (5) nickel foam, (6) copper net, (7) silicone pad, (8) ground electrode, (9) polyethylene tube(gas in), (10) epoxy resin board (2 mm), and (11) drilled hole for screw.

2.3. Preparation of a sampling film for HO* detection

The sampling method is similar to the previous article [22]. To collect HO* radical produced in the plasma reaction, one piece of filter paper was cut to a calculated size (300 mm × 45 mm), then a solution, which was made by 0.3 g salicylic acid dissolving in 10 ml anhydrous ethanol (99.9%), was dripped equably by a injector on this filter paper. After that, the paper was dried and weighed until all the solution was loaded on. The filter film was folded as shown in Fig. 3. Though the reaction of SAL and HO* was a gas–solid interface reaction, sampling film collection efficiency could achieve approx-

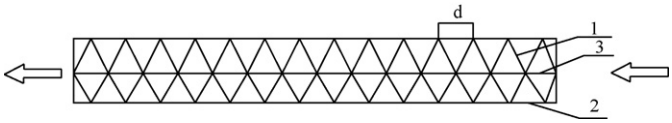

Fig. 3. Position of filter film in the DBD reactor. (1) Filter film; (2) epoxy board; (3) copper net.

imately 100%. The coarse surface of film could easily absorb HO* in the gas stream, and the reaction kinetics between HO* and salicylic acid belonged to the type of diffusion, hence its reaction rate was large [23]. In addition, the method to place the film also favored the effective trapping for its short-range collision.

2.4. HO* analysis system

The analysis method for OH radical was similar to the Ref. [22]. A HPLC (Ultimate 3000, Dionex), which was performed using a C_{18} reversed-phase column (5 m, 250 mm × 4.6 mm) with the column temperature of 35 °C, was used to separate and determine the amount of products and residual SAL. HPLC was run isocritically with a mobile phase consisting of 40% (v/v) methanol, with 60% deionized water at a flow rate of 1 ml/min. The HPLC system coupled with an UV detector was used to monitor SAL and hydroxylated derivatives at 300 nm at the condition above. In the HPLC chromatograph the retention time for 2,5-dihydroxybenzoic acid (2,5-DHBA), 2,3-dihydroxybenzoic acid (2,3-DHBA) and SAL is 5.604 min, 7.525 min and 17.686 min, respectively.

2.5. Catalyst preparation

Impregnation with precursors of catalytically active phases constitutes a classical method to prepare heterogeneous catalysts. In this paper, catalyst of manganese oxide/alumina/nickel foam was prepared with a mass ratio of 50%:50%:100%. The catalyst was prepared by an incipient wetness impregnation method. First a sol of alumina was loaded on nickel foam until the mass ratio was up to 50%:100%, then precursors of $Mn(NO_3)_2$ were deposited on the support. After that, it was dried at 393 K for 2 h, and then calcined at 723 K for 4 h.

2.6. Catalyst characterization

Specific surface area analysis of BET for the catalyst was measured by a surface area analyzer (ASAP 2020M, Micromeritics). The sample (0.1 g) was pretreated with a temperature of 200 °C in a vacuum system for 4 h. Then, N_2 was used as an adsorbate to allow the temperature down to −196 °C when the surface of catalyst was measured.

TPR analysis was carried out by using a micromeritics TPR/TPD (thermocouple particle densitometry) 2900 instrument with a self-assembly thermal conductivity detector (TCD). Sample was pretreated at 400 °C using high-purity Ar (30 ml/min) for 1 h. Then H_2 (100% by volume) was used as a reducing gas with a flow rate of 1 ml/s. The catalyst was heating up to 800 °C at a rate of 10 °C/min. Hydrogen consumption was measured approximately by TCD.

The elemental compositions and their valences on the surface of catalysts were analyzed with XPS using VG Multilab 2000 spectrometer equipped with a hemispherical electron analyzer and Mg Ka radiation source ($h\nu$ = 1253.6 eV). All binding energies are referenced to the C 1s line at 284.6 eV, which provided an accuracy of ±0.48 eV within full scanning of 0–1400 eV. A XPS peak 4.1 software was used for fitting.

The toluene removal efficiency, specific energy density, energy efficiency, carbon dioxide selectivity and concentration of HO* were calculated as follows:

Toluene removal efficiency (η):

$$\eta\ (\%) = \frac{[\text{toluene}]_{\text{in}} - [\text{toluene}]_{\text{out}}}{[\text{toluene}]_{\text{in}}} \times 100 \quad (1)$$

Specific energy density (SED):

$$\text{SED}\ (\text{Wh/m}^3) = \frac{\text{discharge power}\ (\text{W})}{\text{gas flow rate}\ (\text{m}^3/\text{h})} \quad (2)$$

Energy efficiency:

$$\eta_{\text{E}}\ (\text{g/kWh}) = \frac{[\text{toluene}]_{\text{removal}}\ (\text{g/m}^3) \times \text{gas flow rate}\ (\text{m}^3/\text{h})}{\text{input power}\ (\text{kW})} \quad (3)$$

Carbon dioxide selectivity:

$$S_{CO_2}(\%) = \frac{[CO_2]}{[CO_2] + [CO]} \quad (4)$$

The concentration of HO* can be calculated by Eq. (4).

$$C_{\text{OH}}\ (\text{Radicals/cm}^3) = \frac{C_{\text{Total}} \times V_{\text{L}} \times N}{F_{\text{Total}} \times F_{\text{g}} \times t \times \eta \times (1-\alpha)} \quad (5)$$

C_{Total}: hydroxylated derivatives concentration formed during sampling (mol/l); V_{L}: scrubbing solution volume after sampling (l); N: Avogadro's number (6.02×10^{23}); F_{Total}: fraction of main hydroxylated derivatives in total products (assumed to be 100%); F_{g}: air flow rate (ml/min); t: sampling period (min); η: extraction efficiency (supposed to be 100%); α: loss rate of HO* passing the sampling films (set to zero).

3. Results and discussion

3.1. Effect of specific energy density on toluene removal efficiency and HO* formation

Fig. 4 shows the relationship between SED [Wh/m^3] and η_{E} [g/kWh] at room temperature with/without catalyst. As could be seen from the figure, there was a relatively stronger dependence of energy efficiency on SED without catalyst than that with catalyst. For example, when SED increased from 39 Wh/m^3 to 89 Wh/m^3, η_{E} without catalyst ranged from 0.21 g/kWh to 1.12 g/kWh. But with MnO_X catalyst, it only varied from 0.97 g/kWh to 1.18 g/kWh.

Fig. 5 shows that only 2,3-DHBA and 2,5-DHBA were found as hydroxylated derivatives and the amount of 2,3-DHBA was larger than that of 2,5-DHBA. It is possible because the generation of 2,5-DHBA and 2,3-DHBA is effected by the distribution of electron cloud on the benzene ring, the carboxyl and hydroxyl. Moreover, the activity of site 3 is higher than that of site 5 for the conjugative effect of electron.

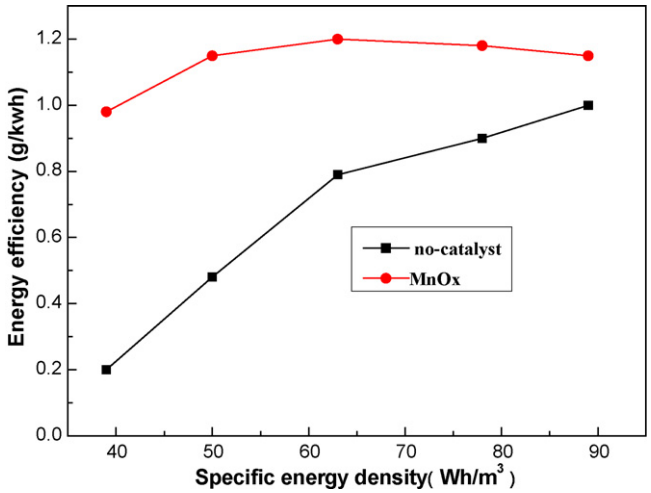

Fig. 4. Effect of SED on energy yield of different catalysts (relative humidity: 20%; toluene initial concentration: 400 mg/m^3; gas flow rate: 450 ml/min).

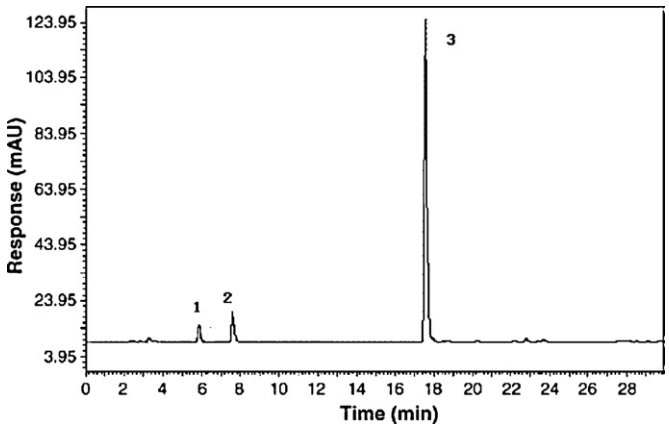

Fig. 5. Chromatograms of 2,5-DHBA, 2,3-DHBA and salicylic acid. The retention time: (1) 5.604 min for 2,5-DHBA; (2) 7.525 min for 2,3-DHBA; (3) 17.686 min for salicylic acid.

Fig. 6(a) shows that toluene removal efficiency increases significantly when MnO_X catalyst is introduced into the discharge area. For example, with the catalyst in situ, the toluene removal efficiency (η) was 64.8% at a SED of 50 Wh/m^3, which was two times more than that of 31.8% without catalyst. It also illustrates that the toluene removal efficiency increased with the increasing of SED whether catalyst exists or not. When SED was regulated from 39 Wh/m^3 to 89 Wh/m^3, η varied from 48.7% to 99.8% with MnO_X catalyst while η of 25.6–95.8% existed without catalyst.

Fig. 6(b) shows that the HO* yield increases with the increase of SED, and the concentration of HO* in gas stream

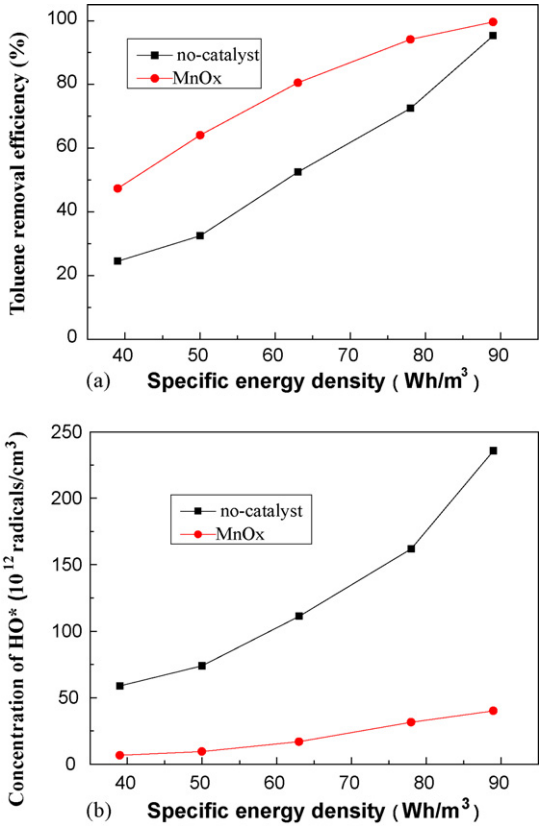

Fig. 6. Effect of specific energy density on the toluene removal efficiency and HO* formation (relative humidity: 20%; toluene initial concentration: 400 mg/m^3; gas flow rate: 450 ml/min).

Table 1
Comparison of HO* yield with/without catalyst at a SED of 62.5 Wh/m^3.

Amount of HO* ($\times 10^{13}$ radicals/cm^3)	Without catalyst	With MnO_X catalyst
In the gas stream	111.38	17.04
On the surface	0	89.14
Total	111.38	106.28

with catalyst is much lower than that without catalyst. The concentrations of HO* without catalyst were in the range of $(5.9–23.6) \times 10^{13}$ radicals/cm^3. But with catalyst, they just varied with $(0.67–4.12) \times 10^{13}$ radicals/cm^3.

Comparing Fig. 6(a) with (b), it was found that there was a parallel trend between the HO* density and toluene removal efficiency without catalyst in gas stream. Though the amount of HO* in gas stream with catalyst was much less than that without catalyst, the toluene removal efficiency was much higher. It is possible that without catalyst an increase in SED would lead to an increase of high-energy electron density. More electron mean energy would cause an increase of oxidative radicals, which was beneficial to the degradation of pollutants. When a catalyst was loaded in situ, less HO* was detected. Maybe it should be ascribed to the adsorption ability of MnO_X catalyst could inhibit the formation of HO*.

To confirm the reason, the quantities of HO* radicals both in the gas phase and on the surface of catalyst have been detected in the plasma-catalysis system. After the catalyst was prepared, salicylic acid solution was dripped evenly onto the surface of the catalyst. Then a same method as the former was used to detect HO*. The results can be seen in Table 1. The table demonstrated that the amount of HO* produced in plasma-catalysis system was nearly equal to that without catalyst. But with catalyst in situ the amount of HO* radicals on the surface of catalyst was 89.14×10^{13} radicals/cm^3, while that of 17.04×10^{13} radicals/cm^3 existed in the gas stream. Therefore the reason that the catalyst could enhanced the toluene removal efficiency may be not due to the amount of HO*, but due to the efficient reaction of HO* with toluene on the surface, or the active sites and other active species on the catalyst. It proves that MnO_X catalyst would adsorb HO* in plasma reaction.

3.2. Effect of relative humidity on toluene removal efficiency and hydroxyl radicals

Water plays a very important role in the reaction since it decomposes into OH and H free radicals inside the plasma system. It is necessary to study the effect of water on the HO* formation with/without catalyst.

From Fig. 7(a) and (b), it could be seen that there was a parallel trend between the HO* density and toluene removal efficiency without catalyst in gas stream at various relative humidities (RH). The highest HO* yield and toluene removal efficiency were achieved with a RH of 20%. However, when water was added to the DBD reactor with catalyst in situ, there was no direct relationship between the quantities of HO* in the gas stream and the toluene removal efficiency. The highest HO* yield was also obtained at a RH of 20%, and there was a fine distinction of HO* yield among various humidities. But the toluene removal efficiency decreased with the increase of humidity when catalyst added. It is possible that water covers on the surface of the catalyst and results in a decrease in the reaction probability.

The highest HO* yield and toluene removal efficiency were achieved with a RH of 20% because of the electronegative characteristic of water. When the humidities ranged from 0% to 20%, with the increasing of RH, more H_2O molecules collide with high-energy electrons and form OH radicals, resulting in a higher removal

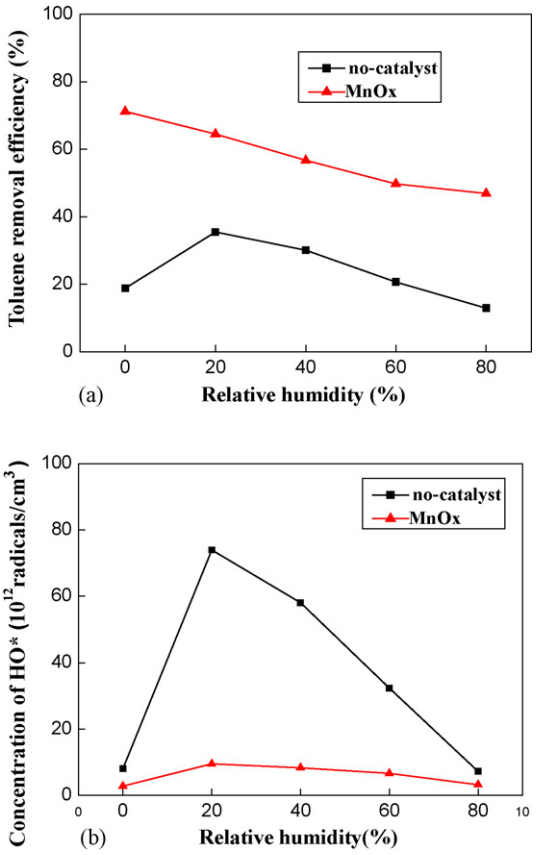

Fig. 7. Effect of relative humidity on (a) toluene removal and (b) hydroxyl radicals (specific energy density: 50 Wh/m^3; toluene initial concentration: 400 mg/m^3; gas flow rate: 450 ml/min.).

efficiency. However, water also has an adverse effect due to its electronegative characteristics. Increasing the humidity limits the electron density in the system and quenches the activated chemical species [24]. So the HO* yield decreased when RH exceeded to 20%.

3.3. Effect of specific energy density on selectivity of CO_2

Fig. 8 indicates that the selectivity of CO_2 decreased with the increasing of SED. This trend was more obvious from the data without catalyst than those with a catalyst. The quantities of active oxygen species increased under a high SED. The active oxygen species enhance the production of CO to a greater extent than that of CO_2. Therefore the CO_2 selectivity decreased with an increase of SED, and it was consistent with the report of Chavadej et al. [25].

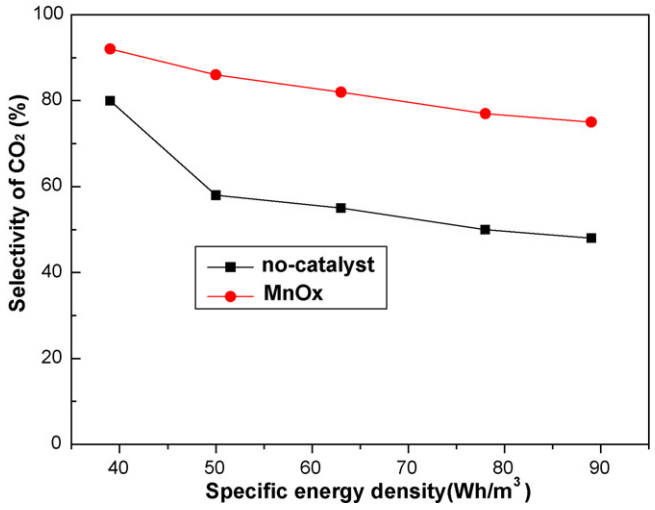

Fig. 8. Influence of specific energy density on the selectivity of CO_2 (relative humidity: 20%; toluene initial concentration: 400 mg/m^3; gas flow rate: 450 ml/min).

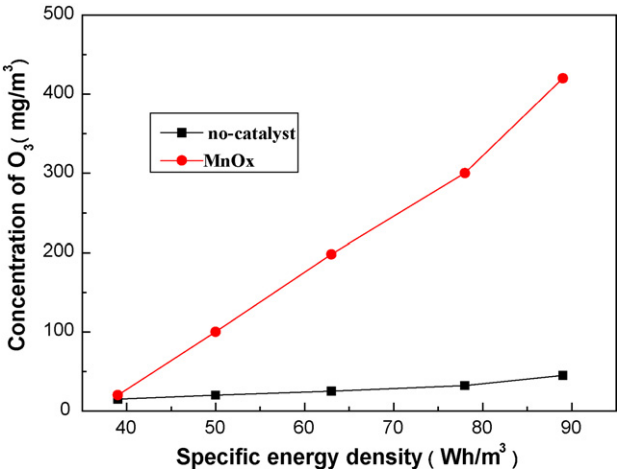

Fig. 9. Influence of specific energy density on the formation of O_3 (relative humidity: 20%; toluene initial concentration: 400 mg/m^3; gas flow rate: 450 ml/min).

Fig. 8 also shows that the selectivity of CO_2 is greatly enhanced by introducing a catalyst into the plasma reaction. Under the same SED of 89 Wh/m^3, the selectivity of CO_2 for DBD reactor was only 48.8% with no catalyst but it increased to 82.6% with the MnO_X catalyst. The selectivity was enhanced with active components due to the toluene oxidation near and/or on the catalyst surface. Maybe this is due to that O active species are formed through the decomposition of O_3 on the surface of catalyst, and O active species would further oxide CO and toluene (or intermediate reaction products) into CO_2. Therefore a higher CO_2 selectivity was achieved [26].

3.4. Effect of specific energy density on byproducts

The formation of byproducts is one of the main problems for removal of VOCs using a plasma system. Ozone, nitrogen oxides, aerosol particles et al are always existed in the reaction. Catalyst combined with plasma was thought to be an effective way to reduce byproducts [2–4]. The composition of aerosol particles is very complicated. These species probably formed carbon deposits, polymers, particulates, and so on. In our group, several other researchers focus on the analysis of aerosol particles. In this paper, ozone and nitrogen oxides as the main byproducts are emphasized.

3.4.1. O_3

Ozone is one of the major byproducts for waste gas treatment with plasma technology. MnO_X catalyst was proved to be effective on ozone decomposing [27]. Fig. 9 shows that with MnO_X catalyst, the concentration of O_3 in the gas stream was much lower than that without catalyst. For example, under a SED of 89 Wh/m^3 the concentration of O_3 was only 34.6 mg/m^3 with MnO_X catalyst, but it increased to 420 mg/m^3 without catalyst. It is due to that ozone is decomposed to oxygen molecules and active oxygen atoms on the surface of catalyst. The result of XPS below was also verified the existence of absorbed oxygen atom.

Radhakrishnan et al. [28] considered that ozone decomposition occurred through an electron transfer from Mn^{n+} to an ozone molecule on the surface of MnO_X. Delagrange et al. [29] presented

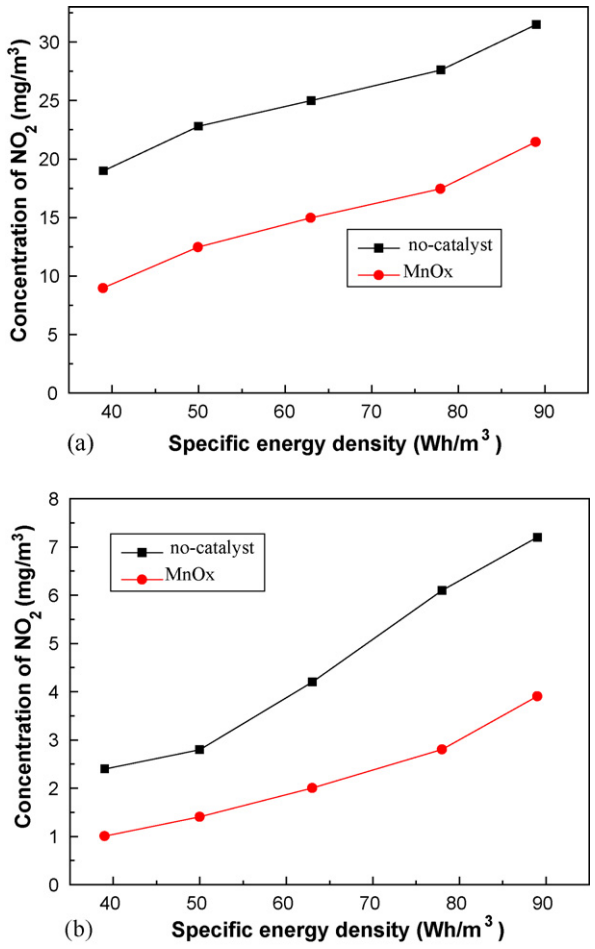

Fig. 10. Effect of specific energy density on the formation of NO_x (a: NO_2; b: NO) (relative humidity: 20%; toluene initial concentration: 400 mg/m^3; gas flow rate: 450 ml/min).

that a mechanism for O_3 decomposition with MnO_X was as follows:

$$O_3 \xrightarrow{MnO_2} O(^3P)+{}^1\Delta O_2 \quad O_3 \xrightarrow{MnO_2} O(^1D)+{}^3\Sigma O_2 \qquad (6)$$

MnO_X/γ-Al_2O_3/nickel foam accelerated the decomposition of O_3 on the surface of catalyst.

3.4.2. NO_x

Fig. 10 shows the concentrations of NO and NO_2 with/without catalyst as the function of input power in the reactor. It indicates that high SED favors the formation of NO_x. Both the concentration of NO and NO_2 increases with the increasing of SED. It also shows that MnO_X catalyst significantly reduces the formation of NO_x. The amount of NO_2 produced in the DBD with catalyst in situ was 9.8 mg/m^3 under the SED of 89 Wh/m^3, which is only half of that without catalyst. This is in agreement with the articles of Park et al. [30] and Kawasaki et al. [31].

Fig. 10 also shows that the concentration of NO in the effluent was much lower than that of NO_2. It is due to that excess of active molecules and radicals such as O_3, OH and O, are effective to oxidize NO into NO_2.

These results may be attributed to the catalysts introduced into the plasma discharge area affecting the nature of discharge or inducing a shift in a distribution of the accelerated electrons. Furthermore, long-lived species produced in interaction of catalyst and plasma could favor the decomposition of toluene on the surface of catalyst [32]. Hence, NO_x may decompose toluene at the catalyst surface and convert to other products. Finally, it is possible that adsorption is another reason for less NO_x production with catalyst. The following results of XPS could support the hypothesis.

Table 2
Comparison of BET surface area of MnO_X catalyst with those catalysts in Ref. [2].

Active components of catalysts	BET surface area (m^2/g)
MnO_X	84.4
CoO_X in Ref. [2]	6.0
CuO_X in Ref. [2]	10.7
FeO_X in Ref. [2]	24.3
MnO_X in Ref. [2]	35.2

3.5. Characterization of catalyst

3.5.1. BET

The BET surface area of the MnO_X catalyst was measured at 84.4 m^2/g. Table 2 shows the comparison of BET surface area of MnO_X catalyst with those catalysts in Ref. [2]. Comparing these data, it was found that manganese oxide owns a much larger BET surface area. Commonly speaking, a higher BET surface area means a higher dispersion of the catalyst and a bigger contact area between active component and gas, which leads to a better catalytic activity. Therefore, manganese oxide catalyst has a good catalytic activity, and this is in good consistent with the results of the plasma-catalytic performances test on toluene decomposition.

3.5.2. XPS

XPS technique is suitable for identifying the various states of species deposited on the catalyst. Fig. 11 shows the complex chemical composition of the MnO_X on the catalyst surface through XPS spectrum. The C 1s region exhibited aromatic/alkanes, aliphatic, and oxygen-bearing carbon.

The survey spectrum was recorded in the binding energy (BE) ranging from 0 eV to 1400 eV. The peak positions corresponding to Mn 2p, O 1s, N 1s and C 1s have been searched in the BE range of 635–660 eV, 528–534 eV, 395–402 eV and 280–288 eV, respectively. The curves obtained have been shown in Fig. 9(a)–(c). The peak position corresponding to Mn^{4+} $2p_{1/2}$ and Mn^{4+} $2p_{3/2}$ are, respectively, 654.8 eV and 642.6 eV, and this result is in good agreement with that given in the article [33].

According to the XPS database and lasurface database, there are three oxygen species on the catalyst surface. A BE at 528.8–529.7 eV was a characteristic peak of lattice oxygen O^{2-}(OL). A weak adsorption of oxygen O^-(OC, A) on the surface falls at a BE of 531.0 ± 0.5 eV. A BE at 532.6 ± 0.5 eV belongs to the adsorbed oxygen molecule O^{2-}(OC, A). The presence of the peak in a BE curve at 654.8 eV is assigned to Mn^{2+}, and 529.0 eV represents lattice oxygen. Therefore XPS studies indicate Mn^{2+} and oxygen in O^{2-} chemical states, and confirms the formation of MnO_X when $Mn(NO_3)_2$ was calcined at 450 °C. In addition, from Fig. 10(c) it could be seen that a small amount of N elements has also appeared on the catalyst surface. The source of N on the catalyst comes from the adsorption of NO_x or N radicals dissociated from N_2 in background gas.

The BE for C 1s was at 282–285 eV and 285–288 eV as shown in Fig. 10(d). According to lasurface database, the BE of 282–285 eV due to the existence of Al–C, C–O–Al, C–H, and 285–288 eV ascribes to C–N, C=O, C–O, C–N or the OH in the air plasma.

3.5.3. TPR

Fig. 12 shows the TPR curves for MnO_X catalysts. Under the experimental conditions, there are two distinct reduction peaks of α (the former) and β (the latter), and the reduction temperature

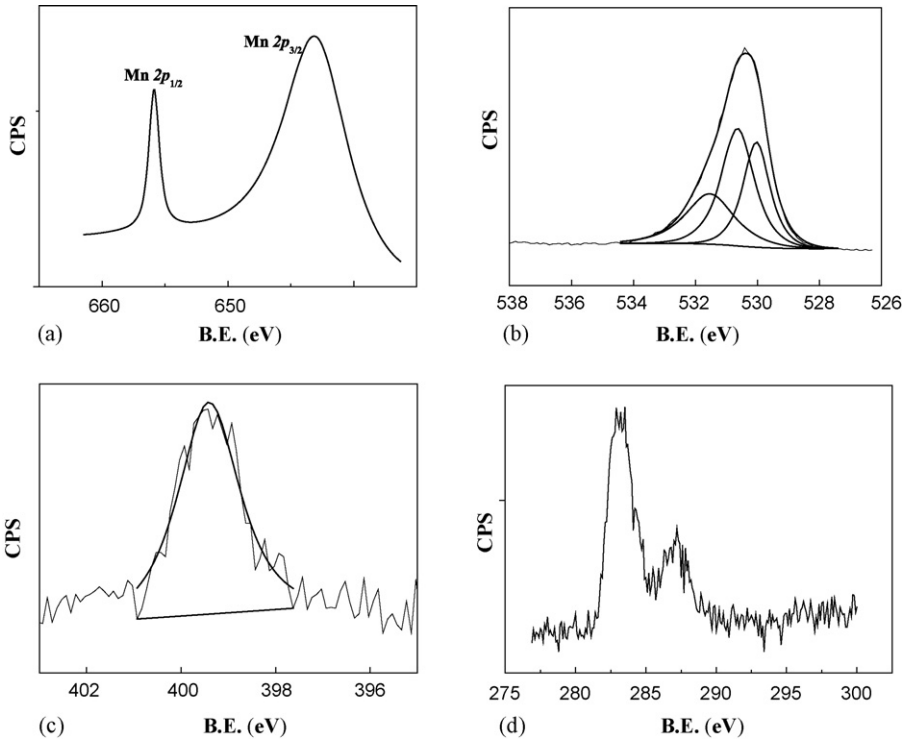

Fig. 11. (a) XPS spectrum of Mn^{4+} 2p, (b) XPS spectrum of O 1s, (c) XPS spectrum of N, and (d) XPS spectrum of C.

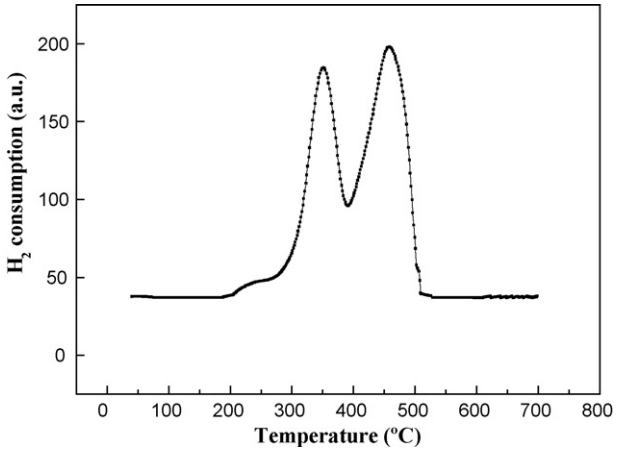

Fig. 12. TPR curves for the MnO_X catalysts.

was 350 °C and 460 °C, respectively. This result is in good agreement with the H_2-TPR results of MnO_X reported in the literature [34].

These two peaks could be attributed to the two-step reduction of MnO_X. The first step corresponds to the reduction of MnO_2 to Mn_3O_4 and the second step is due to the further reduction of Mn_3O_4 to MnO. The reduction of $Mn_3O_4 + H_2 \rightarrow 3MnO + H_2O$ consumes more hydrogen than that of $3MnO_2 + H_2 \rightarrow 2Mn_3O_4 + H_2O$.

4. Conclusions

Toluene removal efficiency increased significantly when MnO_X catalyst was introduced into the discharge area. The concentration of HO* in gas stream with catalyst is much lower than that without catalyst. The quantities of HO* radicals in the gas phase and on the surface of catalyst have been described in a plasma-catalysis system. The quantities of HO* radicals on the surface of catalyst was five times more than that in the gas phase. It proves that HO* would be attached on the surface of catalyst. In addition, the results of XPS also proved that various oxygen species, hydroxyl and some compounds containing N element deposited on the catalyst after plasma reaction. Therefore, combination of non-thermal plasma and catalysts could control the distribution of active oxygen species in situ such as ozone (O_3), oxygen atoms, hydroxyl radical (HO*), and final oxidation products such as CO and CO_2.

Acknowledgements

This work was supported by the National Natural Science Foundation of China (No. 50708021), the Guangzhou University Xinmiao Project (No. gyf1-1001), and the Guangzhou University Scientific Research Startup Project (No. gyf1-1002). In addition, key laboratory of environmental protection and eco-remediation of Guangdong regular higher education institutions was gratefully acknowledged.

References

[1] H.L. Chen, H.M. Lee, S.H. Chen, Y. Chao, M.B. Chang, Appl. Catal. B: Environ. 85 (2008) 1.
[2] Y.F. Guo, D.Q. Ye, K.F. Chen, J.C. He, Catal. Today 126 (2007) 328.
[3] S. Fuamura, A. Zhang, H. Einaga, H. Kabashima, Catal. Today 72 (2002) 259.
[4] W. Mista, R. Kacprzyk, Catal. Today 137 (2008) 345.
[5] M.B. Chang, H.M. Lee, Catal. Today 89 (2004) 109.
[6] H.-H. Kim, S.-M. Oh, A. Ogata, S. Futamura, Appl. Catal. B: Environ. 56 (2005) 213.
[7] T. Oda, J. Electrostat. 57 (2003) 293.
[8] R.D. Bach, O. Dmitrenko, J. Am. Chem. Soc. 128 (2006) 1474.
[9] W.J. Bian, X.L. Ying, J.W. Shi, J. Hazard. Mater. 162 (2009) 906.
[10] S. Kanazawa, T. Ito, Y. Shuto, T. Ohkubo, Y. Nomoto, J. Mizeraczyk, IEEE Trans. Ind. Appl. 37 (2001) 1663.
[11] S. Kanazawa, Y. Shuto, N. Sato, T. Ohkubo, Y. Nomoto, J. Mizeraczyk, J.S. Chang, IEEE Trans. Ind. Appl. 39 (2003) 333.
[12] G.J. Roth, M.A. Gundersen, IEEE Trans. Plasma Sci. 27 (1999) 28.
[13] H. Hazama, M. Fujiwara, M. Tanimoto, Chem. Phys. Lett. (2000) 542.
[14] F. Fresnet, G. Baravian, S. Pasquiers, C. Postel, V. Puech, A. Rousseau, M. Rozoy, J. Phys. D: Appl. Phys. 33 (2000) 1315.
[15] F. Tochikubo, T. Watanabe, Hakone VII 1 (2000) 219.

[16] A. Ershov, J. Borysow, J. Phys. D: Appl. Phys. 28 (1995) 68.
[17] R. Ono, T. Oda, J. Electrostat. 55 (2002) 333.
[18] F. Tochikubo, S. Uchida, T. Watanabe, Jpn. J. Appl. Phys. 43 (2004) 315.
[19] S. Kanazawa, H. Tanaka, A. Kajiwara, T. Ohkubo, Y. Nomoto, M. Kocik, J. Mizeraczyk, J.-S. Chang, Thin Solid Films 515 (2007) 4266.
[20] L. Magne, S. Pasquiers, C. R. Phys. 6 (2005) 908.
[21] Z. Machala, M. Janda, K. Hensel, I. Jedlovsky, L. Leštinska, V. Foltin, V. Martisovits, M. Morvova, J. Mol. Spectrosc. 243 (2007) 194.
[22] Y.F. Guo, X.B. Liao, D.Q. Ye, J. Environ. Sci.-China 20 (2008) 1429.
[23] X. Ren, K. Shao, G. Miao, China Environ. Sci. 21 (2001) 115.
[24] S. Futamura, T. Yamamoto, IEEE Trans. Ind. Appl. 33 (1997) 447.
[25] S. Chavadej, W. Kiatubolpaiboon, P. Rangsunvigit, T. Sreethawong, J. Mol. Catal. A 263 (2007) 12.
[26] S. Chavadej, K. Saktrakool, P. Rangsunvigit, L.L. Lobban, T. Sreethawong, Chem. Eng. 132 (2007) 345.
[27] H.B. Huang, D.Q. Ye, X.J. Guan, Catal. Today 139 (2008) 43.
[28] R. Radhakrishnan, S.T. Oyama, Y. Ohminami, J. Phys. Chem. B 105 (2001) 9067.
[29] S. Delagrange, L. Pinard, J.M. Tatibouet, Appl. Catal. B: Environ. 68 (2006) 92.
[30] S.Y. Park, B.R. Deshwal, S.H. Moon, Fuel Process. Technol. 89 (2008) 540.
[31] T. Kawasaki, S. Kanazawa, T. Ohkubo, J. Mizeraczyk1, Y. Nomoto, Thin Solid Films 386 (2001) 177.
[32] V. Cooray, M. Rahman, J. Electrostat. 63 (2005) 977.
[33] L.J. Yuan, Z.C. Li, J.T. Sun, K.L. Zhang, Y.H. Zhou, Mater. Lett. 57 (2003) 1945.
[34] A. Chen, H.L. Xu, Y.H. Yue, W.M. Hua, W. Shen, Z. Gao, J. Mol. Catal. A: Chem. 203 (2003) 299.